Optical Pulling Force in Non-Paraxial Bessel Tractor Beam Generated with Polarization-Insensitive Metasurface

Zhe Shen(沈哲)* and Xin-Yu Huang(黄昕宇)

School of Electronic and Optical Engineering, Nanjing University of Science and Technology, Nanjing 210094, China

(Received 17 February 2023; accepted manuscript online 10 April 2023)

Tractor beams, able to produce optical pulling forces (OPFs) on particles, are attracting increasing attention. Here, non-paraxial Bessel tractor beams are generated using polarization-insensitive metasurfaces. OPFs are found to exert on dielectric particles with specific radii at the axes of the beams. The strengths of the OPFs depend on the radii of the particles, which provides the possibility of sorting particles with different sizes. For the OPFs, the radius ranges of particles vary with the polarization states or topological charges of the incident beams. The change of polarizations can provide a switch between the pulling and pushing forces, which offers a new way to realize dynamic manipulation of particles. The change of topological charges leads to disjoint radii ranges for the OPFs exerting on particles, which provides the possibility of selective optical separation. Moreover, we study the behaviors of particles in the tractor beams. The simulation results reveal that linearly or circularly polarized tractor beams can pull particles a sufficient distance towards the light source, which verifies the feasibility of separating particles.

DOI: 10.1088/0256-307X/40/5/053701

Since Galileo discovered that a comet's tail always points away from the sun, researchers have realized that light can exert force on an object.[1] Not only a beam can push an object forward,[2] but other "trapping",[3,4] "pulling",[5] "rotating",[6] and "spinning"[7] functionalities were also developed as the basic modes of modern optical micromanipulation for particles. These micromanipulation modes are widely used in biology,[8] chemistry,[9] manipulation, and assembly of nanostructures.[10] Among all the developed manipulation modes, optical pulling has attracted widespread attention.[11–14] The optical force directed to the light source is called optical pulling force (OPF). Although it seems counterintuitive, OPF has been theoretically verified[15] and experimentally demonstrated[16] in recent years. The discovery of OPF provides a new degree of freedom for optical manipulation technology.[17] Nowadays, researchers have developed various methods to generate beams to obtain OPF, and we call those beams the "tractor beams". In general, these methods can be divided into two categories: the first category uses some special properties of the target or environmental medium to passively pull the target particles. This kind of method includes obtaining OPFs with objects with exotic object parameters, such as the optical gain medium structures[18] or chiral objects,[12] and designing special background mediums.[19,20] The second category directly utilizes light to actively pull particles. For example, the interference of multiple beams, such as Gaussian beams[16] or plane waves,[14] can exert OPFs on particles. A single structured beam, such as an optical solenoid beam[21,22] or a non-paraxial Bessel beam,[11,23] can also exert OPFs on objects.

Employing a single non-paraxial Bessel beam is a typical method to obtain OPFs on particles. So far, general Bessel beams have been applied in particle sorting,[24,25] and non-paraxial Bessel beams have the potential to achieve sorting in a more unique way. Therefrom, cells with different sizes and refractive indexes can be trapped at diffraction rings of different orders of the Bessel beam, and sorted out with microcapillaries. It has been reported that the optical forces on particles in non-paraxial Bessel beams are related to the size of the particles,[26] which indicates the potential for separation of particles. In addition, according to the theoretical formulas,[27] the optical forces in the propagation direction near the optical axis are much larger than those in the lateral direction, which let the Bessel beam have the possibility of large-angle sorting. Thus, it is highly desirable to generate non-paraxial Bessel tractor beams for exploration of particle separation.

In practical applications, to generate a Bessel beam, the common traditional method is to use a conical lens[28] or a spatial light modulator.[29] Modulating a Bessel structured beam also requires other complex components, which makes the entire optical system huge and complicated. Metasurface is an element composed of subwavelength units. The complexity of the system is greatly simplified with the aid of metasurfaces. It can flexibly adjust the local phase, and it can also integrate the functions of multiple devices on a single monolithic structure. For example, adding additional phase gradients[30] and the vortex phase[31] to the focused beam, or changing the phase distribution to achieve special intensity distribution of the beam,[32] using only a monolithic structure. Such a feature provides more possibilities for light field manipulation.[33–36] Therefore, it is a suitable method to generate non-paraxial Bessel tractor beams with metasurfaces.

In this Letter, we propose a method to generate non-

*Corresponding author. Email: shenzhe@njust.edu.cn
© 2023 Chinese Physical Society and IOP Publishing Ltd

paraxial Bessel tractor beams by polarization-insensitive metasurfaces. It is expected to exert OPFs on particles in tractor beams rather than depending on the background medium around the particles. The polarization-insensitive metasurfaces are used to serve the incidence of different polarizations so that we can study the polarization effects on the OPFs. In addition, we analyze the behaviors of particles under OPFs and explore the possibility for optical sorting. Lastly, we study the influence of topological charges on the OPF. The proposed setup of metasurfaces is not just limited to generating a tractor beam, they have great potential in applications to separate micro-particles with different radii on chip.

Theory Basis about Optical Pulling Force. The optical force is related to the radiation force cross-section of a particle in a beam. The OPF is determined by the optical force component along the propagating direction. Thus, the optical force on a particle along the propagating direction is discussed only. Considering the case of the dielectric particles placed at the propagation z axis, the optical force along the z-axis can be written as[26]

$$\boldsymbol{F}_z^u = \left(\frac{n_{\text{ext}}}{c}\right) I_0 C_z^u \boldsymbol{e}_z, \tag{1}$$

where I_0 is the beam intensity, n_{ext} is the refractive index of the exterior medium surrounding the sphere, and $\boldsymbol{e}_z$ denotes the unit vector pointing in the propagating z direction. The parameter C_z^u is the radiation force cross-section along the z-axis, and u denotes the polarization of the beam.

Vector spherical wave functions (VSWFs) are used to calculate the cross-section. Since the particles used in the simulations are uniform, the optical force remains unchanged under linearly polarized beams with different polarization directions. A circularly polarized light can be decomposed orthogonally into two linearly polarized beams, and the optical force it exerts is equal to the force generated by a linearly polarized beam. Here we only need to discuss circumstances under a linearly polarized beam.

For uncharged dielectric particles in vacuum whose size is smaller than the wavelength of the incident beams, the radiation force cross-section C_z^u can be given as[26]

$$\begin{aligned} C_z^u = & \frac{\lambda^2}{\pi}\text{Re}\Big\{\sum_{n=1}^{\infty}\frac{1}{n+1}(A_n g_{n,\text{TM}}^{0,u} g_{n+1,\text{TM}}^{0,u^*} + B_n g_{n,\text{TE}}^{0,u} g_{n+1,\text{TE}}^{0,u^*}) \\ & + \sum_{v=1}^{n}\Big[\frac{1}{(n+1)^2}\frac{(n+v+1)!}{(n-v)!}(A_n g_{n,\text{TM}}^{v,u} g_{n+1,\text{TM}}^{v,u^*} \\ & + A_n g_{n,\text{TM}}^{-v,u} g_{n+1,\text{TM}}^{-v,u^*} + B_n g_{n,\text{TE}}^{v,u} g_{n+1,\text{TE}}^{v,u^*} \\ & + B_n g_{n,\text{TE}}^{-v,u} g_{n+1,\text{TE}}^{-v,u^*}) \\ & + v\frac{(2n+1)}{n^2(n+1)^2}\frac{(n+v)!}{(n-v)!} \\ & \cdot C_n(g_{n,\text{TM}}^{v,u} g_{n,\text{TE}}^{v,u^*} - g_{n,\text{TM}}^{-v,u} g_{n,\text{TE}}^{-v,u^*})\Big]\Big\}. \end{aligned} \tag{2}$$

In order to ensure adequate convergence, $n_{\max} = kr + 4(kr)^{1/3} + 10$. Here r denotes the radius of particles, and k is the wave number. Parameters A_n, B_n, and C_n can be written as

$$\begin{aligned} A_n &= a_n + a_{n+1}^* - 2a_n a_{n+1}^*, \\ B_n &= b_n + b_{n+1}^* - 2b_n b_{n+1}^*, \\ C_n &= -i\left(a_n + b_{n+1}^* - 2a_n b_{n+1}^*\right), \end{aligned} \tag{3}$$

where a_n and b_n are the nth order Mie scattering coefficients, which can be inquired in Ref. [37]. The parameters $g_{n,\{\text{TM,TE}\}}^{v,u}$ are the beam-shape coefficients (BSCs), which change with the polarization of the beam, and BSCs of beams with different polarizations can be inquired in Ref. [26]. The parameter u indicates the polarization state of the incident beam. This allows us to theoretically study the polarization effect of OPFs.

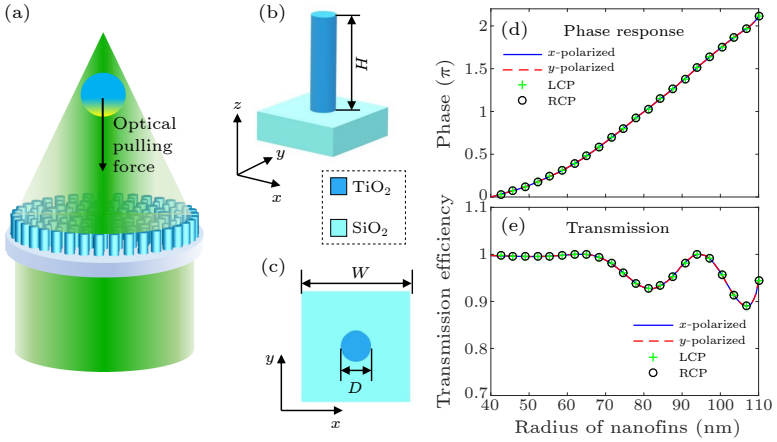

Fig. 1. (a) Schematic diagram of the system. (b) Schematic diagram of the unit. H is the height of the element, and $H = 600\,\text{nm}$. (c) The x–y cross-sectional view of the unit. W is the width of the unit, and $W = 250\,\text{nm}$. D is the diameter of the nanofins. [(d), (e)] The phase shift and the transmission efficiency of nanofins with different radii, with the incident beams of x-polarized, y-polarized, left-handed circularly polarized (LCP), and right-handed circularly polarized (RCP) beams, respectively.

Design Method of the Metasurfaces. The metasurface is composed of TiO_2 cylindrical nanofins of subwavelength size on a SiO_2 substrate, as shown in Fig. 1(a). Compared to silicon-based materials, the TiO_2 material has lower intrinsic loss in visible range (400–700 nm).[38] The plane waves are incident from the direction of the sub-

strate, transmit through the metasurface, and generate non-paraxial Bessel beams. Next, the non-paraxial Bessel beams shine on the particle, and can exert optical forces on the particle. In order to use these nanofins to form lenses, cylinders with different radii should be able to change the phase of incident beams in the range of 0–2π. The phase shifts caused by the cylinders of different diameters are simulated with the incident beams of x-polarization, y-polarization, left-handed circularly polarization, and right-handed circularly polarization, respectively. The wavelength of the beams is 532 nm. As shown in Fig. 1(d), nanofins meet the requirements of phase modulation when their radii change from 40 nm to 110 nm. The four cases maintain the same phase control. It can be seen from Fig. 1(e) that the transmission efficiency is high with all four incident beams. These consistent results demonstrate that the metasurface can ensure a phase polarization-insensitive response.

To generate a Bessel beam, the phase distribution of the metasurface needs to conform to the phase distribution of the axicon lens. For an arbitrary point $P(x, y)$ on the surface of the lens, the phase distribution $\Psi_{\text{Bessel}}(x, y)$ should satisfy the equation

$$\Psi_{\text{Bessel}}(x, y) = -\frac{2\pi}{\lambda}\sqrt{x^2 + y^2}\sin\alpha, \tag{4}$$

where λ is the wavelength of the incident beam in vacuum, and α is the convergence angle of the Bessel beam. The phase of the optical vortex (OV) reads

$$\Psi_{\text{OV}}(x, y) = \begin{cases} m \cdot \arctan(y/x), & x > 0, \\ m \cdot [\arctan(y/x) + \pi], & y \geqslant 0,\ x < 0, \\ m \cdot [\arctan(y/x) - \pi], & y < 0,\ x < 0, \\ m \cdot (\pi/2), & y > 0,\ x = 0, \\ m \cdot (-\pi/2), & y < 0,\ x = 0, \\ \text{undefined}, & y = 0,\ x = 0, \end{cases} \tag{5}$$

where m is the topological charge of the OV. The phase distribution of a high-order Bessel beam reads

$$\Psi_{\text{Bessel}}(x, y) = \Psi_{\text{OV}}(x, y) - \frac{2\pi}{\lambda}\sqrt{x^2 + y^2}\sin\alpha. \tag{6}$$

According to previous work, when the convergence angle of a Bessel beam is small (typically smaller than 60°), there is almost no pulling force on the particles in the beam.[11,26] OPFs can only be observed if the convergence angle is large enough. In this study, to generate non-paraxial Bessel beams, we take $\alpha = 70°$. In order to follow the shape of the phase stripes, the arrangement of the cylinders takes a circular formation. The process to fabricate the TiO_2 nanofins employs the atomic layer deposition (ALD).[38] First, the electron-beam carves the patterns on the resist. Then, TiO_2 can be deposited on the carved resist with ALD. Finally, the required nanofins can be fabricated after the redundant TiO_2 and resist are removed.

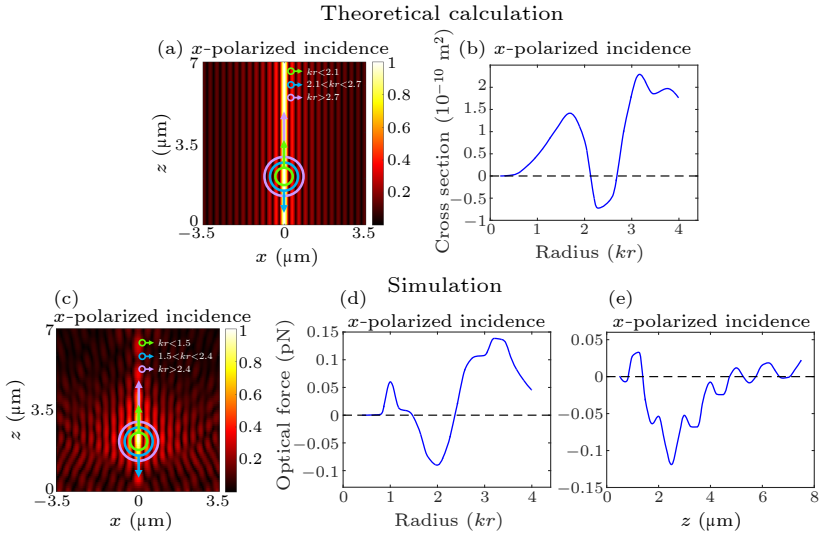

Fig. 2. (a) Magnitude of the normalized electric field distribution of an ideal Bessel beam with theoretic calculation. (b) Radiation force cross-sections in the z direction of particles with different radii. (c) The magnitude of normalized electric field distribution of the Bessel beam generated with the metasurface. (d) Optical forces in the z direction exerting on particles with different radii for the incident x-polarized beam. (e) Optical forces in the z direction on the particles at different positions on the z-axis. The circles of different colors represent particles of different sizes, while the arrows represent forces. It should be noted that their materials are still the same.

Simulation Results of Optical Forces on Particles. In order to investigate the features of optical forces in non-paraxial Bessel beams on particles, we first generate the beams with the polarization-insensitive metasurfaces designed above in simulations, which are performed with the finite difference time domain (FDTD) method with the software Lumerical FDTD. The metasurfaces applied in the simulation are round, and their radii are 10 μm. The plane wave power irradiated on the metasurface is 0.01 W. Particles were placed in the beams generated with the metasurfaces to measure the optical forces on them. The refractive index of the particles is 1.55. In the simulation, the system was set in vacuum. The value of the OPF directed to the light source is negative, and the value of the pushing force is positive.

Influence of the Change of Particle Radii on Optical

Forces. We first theoretically calculate the radiation force cross-sections of the particles at the optical axis in an ideal Bessel beam. According to Eq. (1), the optical forces are proportional to the radiation force cross-section, and the area where the cross-section is negative means that OPFs will be generated. The polarization direction of the beam is along the x-axis, as shown in Fig. 2(a). It is revealed in Fig. 2(b) that the optical force is sensitive to the radius of the particle, and OPFs are observed on the particles with radii between $kr = 2.1$ and 2.7, while particles of larger or smaller sizes were pushed away from the source, as shown in the diagram of optical forces in Fig. 2(a). Here kr is a dimensionless value obtained by product of k (nm^{-1}) and r (nm). Next, we employ the simulation to obtain the optical forces on the particles in the non-paraxial Bessel beams generated with the metasurface. With the software, the data of distribution of the electric field on the desired plane can be obtained with the monitor. Maxwell stress tensor analysis groups can be arranged around particles in the model to calculate the optical forces. Considering that the beam is not tightly focused, the polarization state of the outgoing beam is still consistent with the polarization of the incident beam. In comparison of Figs. 2(a) and 2(c), the length of the non-paraxial Bessel beams generated with the metasurface is limited, and the particles were placed at the position with the highest intensity. As shown by the circles in Fig. 2(c), the particles are set at $z = 2.2\,\mu\mathrm{m}$. It can be seen from Fig. 2(d) that the pulling forces exert on the particles with radii around $kr = 2$, and the peak of pulling forces shifts a little to a smaller radius range. This result confirms that the non-paraxial Bessel beam generated by the metasurface is able to generate forces directed towards the source on the particles, the so-called OPFs. We also study the distance over which the beam can produce OPFs on particles along the propagation direction of the beam. The particle with radius of $kr = 2$ is set on the axis, and we simulate the optical force along the z-axis on the particle when the z-coordinate of the particle changes. As shown in Fig. 2(e), at less than $z = 5\,\mu\mathrm{m}$, the pulling force is observed. The results show that the radii of the particles affect whether the optical force produced by the non-paraxial Bessel beam on the particle is a pulling or pushing force, which let particles of different sizes have different motion trends. In addition, the OPFs can be obtained over a large z-axis range. This enables particle manipulation at a distance from the metasurface, avoiding contamination of target particles by contact. Such features indicate the possibility of particle sorting according to particle sizes.

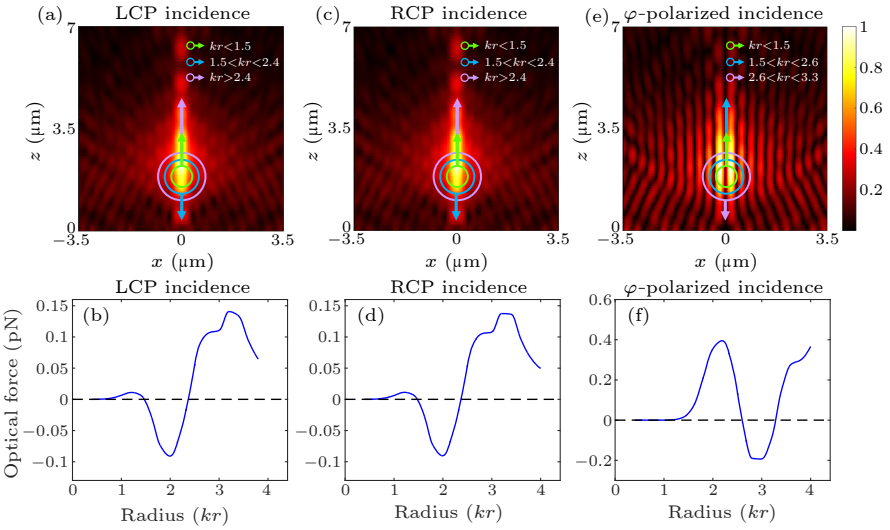

Fig. 3. [(a), (c), (e)] The x–z cross-sectional views of the magnitude of the normalized electric field distribution of non-paraxial Bessel beam generated LCP, RCP and φ-polarized beams. [(b), (d), (f)] The optical forces in the z-direction on particles of different radii. The circles of different colors represent particles of different sizes, while the arrows represent forces. It should be noted that their materials are still unchanged.

Optical Forces under Different Polarizations. Incident beams with different polarization states have an impact on the optical forces on particles as revealed in the previous work.[26] With the polarization-insensitive metasurface, incident beams with LCP, RCP, and azimuthal polarization (φ-polarized) were chosen to study the influence of the polarization on the OPF. In the previous work,[26] under conditions similar to those set by us, due to the strong longitudinal component of the beam, particles experience little pulling forces. Hence, this situation is not discussed here. The particles are placed at the optical axis, and we obtain the optical forces on particles of different radii. It can be seen from Figs. 3(a), 3(c), and 3(e) that the x–z sections of beams generated with the LCP and RCP beams are almost the same, while the x–z section of the beam generated with the φ-polarized beam splits into two bright lines. It is due to the fact that the φ-polarized Bessel beams become hollow in the x–y section. It should be noted again that the polarization insensitivity refers to the phase polarization insensitivity. Under different polarized incident beams, the distributions of light fields may differ. As illustrated by the curves in Figs. 3(b), 3(d), and 3(f), an incident beam only produces OPFs on particles of specific radii regardless of the polarization. Under circularly polarized beams, the curve of the optical forces also forms a peak around radii of $kr = 2$, where OPFs are ap-

plied to particles. When a φ-polarized beam is incident, particles with radii of around $kr = 3$ are pulled. The φ-polarized Bessel beam is hollow and little light shines on small-sized particles, and it exerts pulling forces on larger particles compared with a circularly polarized beam. According to Figs. 3(b), 3(d), and Fig. 2(d), the circularly polarized and linearly polarized beams both exert OPFs on particles of radii around $kr = 2$, and the ranges of the pulling forces are almost the same. These results show that non-paraxial Bessel beams generated by the metasurface can exert OPFs on particles with the incident beams of different polarizations. The pulling forces are sensitive to the radii of the particles, which offers the possibility of the particle sorting based on size. The change of polarization of the beam can achieve different pulling or pushing effects on particles, and the regions of OPFs are disjoint under beams with different polarizations. Obviously, for a particle with radius around $kr = 2$ [e.g., the blue particles in Figs. 3(a) and 3(e)], the change of polarizations from linear or circular polarization to azimuthal polarization, the beam provides a switch from a pulling force to a pushing force. The result indicates the selective optical pulling controlled by the polarization of the beam. Such a feature indicates the possibility of optical dynamic manipulation of nanoparticles.

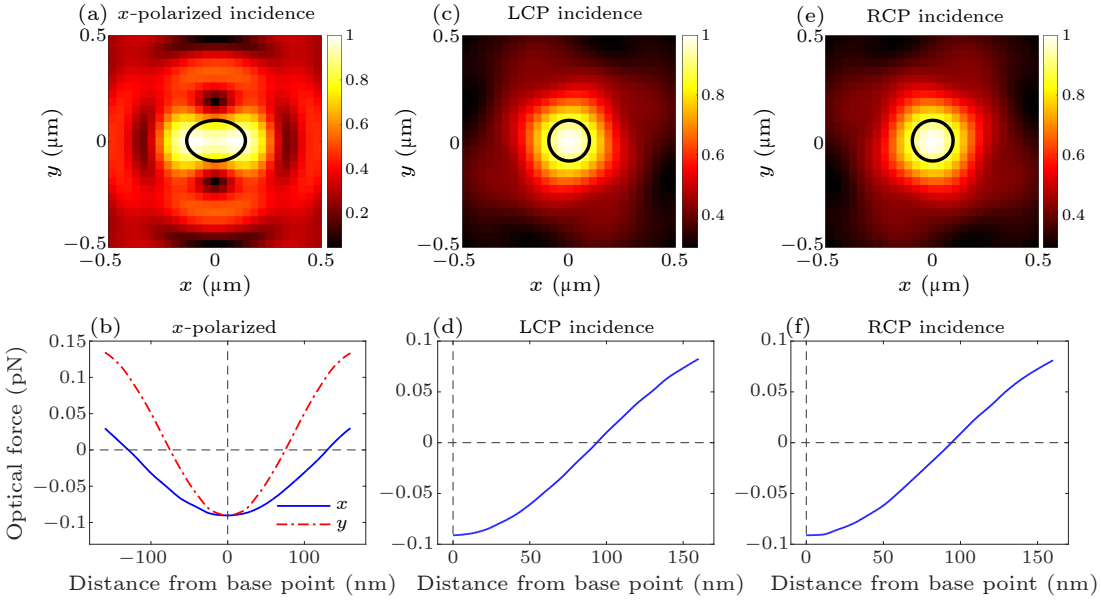

Fig. 4. [(a), (c), (e)] Particles with a radius of $kr = 2$, located on the z-axis at $z = 2.2\,\mu$m. The black circles show the approximate zone of OPFs. The incident beams are x-polarized, LCP, and RCP beams, respectively. The zone of OPFs exerting on particles is simulated. [(b), (d), (f)] Optical forces along z direction on particles at different positions in the $z = 2.2\,\mu$m plane.

To investigate the lateral shape of the location where the OPFs are generated, the particle with a radius of $kr = 2$ is set at different positions in the $z = 2.2\,\mu$m plane with the circularly and linearly polarized incident beams. Through the simulation, we obtain the optical force on the particle at different positions, and we can characterize the shape of the area where the particle is affected by OPF. As shown in Figs. 4(a) and 4(b), when a linearly polarized beam is incident, the particle with a radius of $kr = 2$ is affected by OPF in an ellipse area with the same major axis as the polarization direction. As shown in Figs. 4(c) and 4(e), when an LCP or RCP beam is incident, the areas becomes circular. Therefrom, a circularly polarized beam produces a circular focal spot, while a linearly polarized beam produces a prolate spot.[39] The dark red areas in Figs. 4(c) and 4(e) are symmetrical with each other, which is also consistent with the opposite rotations of the two circularly polarized incident beams. From the curves in Figs. 4(d) and 4(f), the region of OPFs on particles in the beam is almost the same. As the polarization changes, the beams exert OPFs on the particles in regions of different shapes. Such a feature may affect the scope of the OPF when the setup is used in on-chip object transportation or optofluidic devices. These simulations of the scope of the OPFs can provide some reference for manipulating or sorting particles with non-paraxial Bessel beams.

Optical Forces with Different Topological Charges. The topological charges of the incident beams affect the optical forces on particles under beams as well.[26] The metasurface has the ability to flexibly adjust the phase locally, and the vortex phases are added to the lens to investigate the effect of topological charges of beams on the optical force. LCP and RCP beams, with topological charges $m = 1$ and -1, respectively, are employed in the simulations. The particles are fixed on the optical axis. Figures 5(a)–5(c) and 5(d)–5(f) show the particles under OPFs in the Bessel beam generated with LCP beams and RCP beams, respectively. The spin angular momentums (SAMs) of circularly polarized beams are coupled with the orbital angular momentums (OAMs), so different light fields are generated under two topological charges. The SAMs of circularly polarized light with different rotation directions are opposite. Therefore, the light field obtained by the LCP beam at $m = 1$ is similar to that obtained by the RCP beam

at $m = -1$. As shown in Figs. 5(c) and 5(f), compared with the peak of the OPFs in the beam without vortex, the values of OPFs are reduced. Meanwhile, the negative peaks of the curves of the optical forces shift to larger zones when the topological charges are added to the metasurfaces, and beams exerting pulling forces on particles with larger radii. In summary, when topological charges change, both the LCP and RCP beams exert OPFs on particles of different disjoint radius ranges. That is, the radius range allowing for OPFs exerted by the beam with a certain topological charge is approximately the complement of those with other topological charges. Therefore, by changing topological charges for the metasurfaces, the requirement for pulling target particles with certain radii could be satisfied. These results indicate the possibility of a new method to realize size-selective optical pulling of particles with different topological charges.

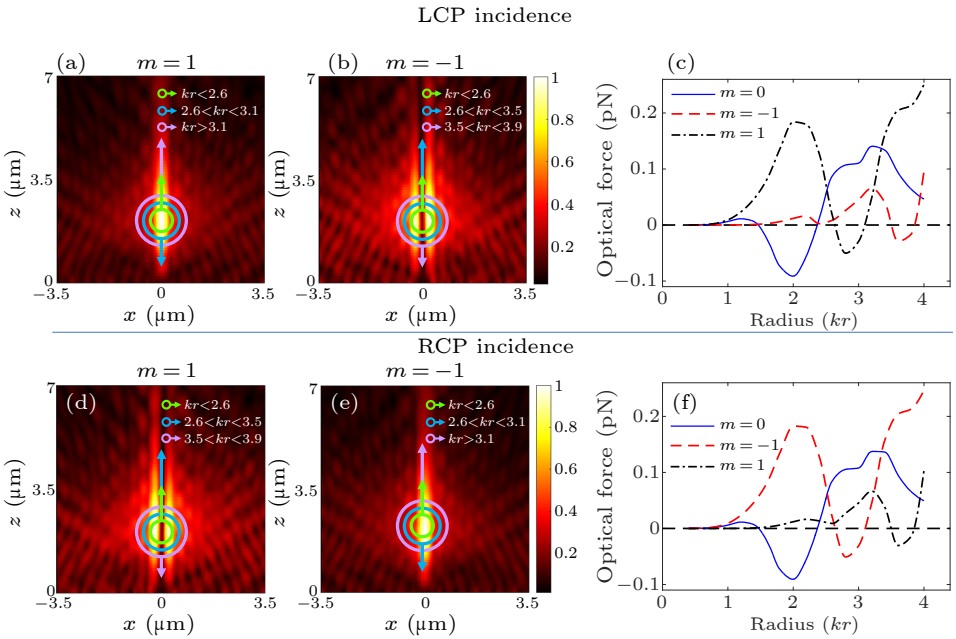

Fig. 5. [(a), (b)] and [(d), (e)] The x–z cross-sectional views of the magnitude of the normalized electric field distribution of the beam generated with an LCP beam and an RCP beam with the topological charge of 1 and -1, respectively. [(c), (f)] The optical forces along z direction exerting on particles of different radii with the beam generated with an LCP beam and an RCP beam, respectively. The circles of different colors represent particles of different sizes, while the arrows represent forces. It should be noted that their materials are still the same.

Trajectories of Particles in the Tractor Beam. The above discussions focus on the case that the particles are placed on the optical axis of the Bessel beam. When the particles are on-axis, particles are not affected by lateral forces due to symmetry. In fact, it is more common for particles not to be on the optical axis. To further observe the effect of optical forces on particles, we study the movement behavior of the particles when they are located slightly off the optical axis with the incidence of LCP and x-polarized tractor beam with simulation, respectively. The particles with radii of $kr = 2$ are set at the point (5 nm, 5 nm) in vacuum. Optical forces on particles at different positions are calculated with simulation, and the particle displacement in a very short time is calculated using Newton's formula. With a loop script, the trajectories are obtained by accumulating the displacements. In the simulations, we assume that the light field of the beam propagates and is unchanged in the z direction. The particles follow different trajectories within the two kinds of beams. Figures 6(a) and 6(b) show the trajectories of the particles in both the cases in the x–y cross-sectional view. As shown in Fig. 6(a), when a circularly polarized beam is incident, the trajectory of the particle is a spiral arc, and the particle quickly falls out of the range of the beam. The situation is different when the beam is converted to a linearly polarized beam. Figure 6(b) shows that the particle stays near the center for a longer period of time. Figures 6(c) and 6(d) show the displacements of particles along the z-axis over time with the two beams, respectively. The two beams have the ability to pull the particle towards the source. Interestingly, although the particle spins away from the center with the incidence of a circularly polarized beam, the particles in it move faster and longer towards the source. Initially near the center, the particle gains a velocity pointing to the source, then the particle quickly spin away from the center, and the intensity of the beam at the edge is too low to generate sufficient pushing force to change the direction of the particle's velocity. These results demonstrate that for a particle of radius $kr = 2$, the tractor beams can pull it a sufficient distance towards the light source. This phenomenon distinguishes it from larger or smaller particles which are pushed by the beam. Such a feature allows the beam to classify particles based on their radii. The results verify the feasibility of the system for particle sorting. Compared with a circularly polarized beam, a linearly polarized beam may help to control the lateral range of motion of particles.

Considering that the angular momentum carried by

the higher-order non-paraxial Bessel beam will affect the movement of particles, the trajectories of particles in tractor beams of different topological charges are studied. We perform the simulations in the LCP beams with topological charges of ± 1. It should be noted that to make sure the particles under OPFs, the radius of particles utilized in the two cases is different ($kr = 2.8$ in the beam with $m = 1$ and $kr = 3.6$ in the beam with $m = -1$). As shown in Fig. 6(e), the particle in the beam with $m = 1$ hovers near the starting point, while in the beam with $m = -1$, the particle races away from the center of the beam, which also appears in Fig. 6(f). In the beam with $m = 1$, OAM and SAM are in the opposite directions. The x–y cross section of the beam presents a light spot. Similar to the linearly polarized beam without angular momentum, particles are tied near the beam center. Also noticeably, in the beam with $m = -1$, the particles are driven quickly away from the center of the beam. It can be concluded that, although the circularly polarized tractor beam cannot stably tie particles near the beam center, applying appropriate vortex phase can better control the lateral movement of particles on the basis of maintaining OPFs.

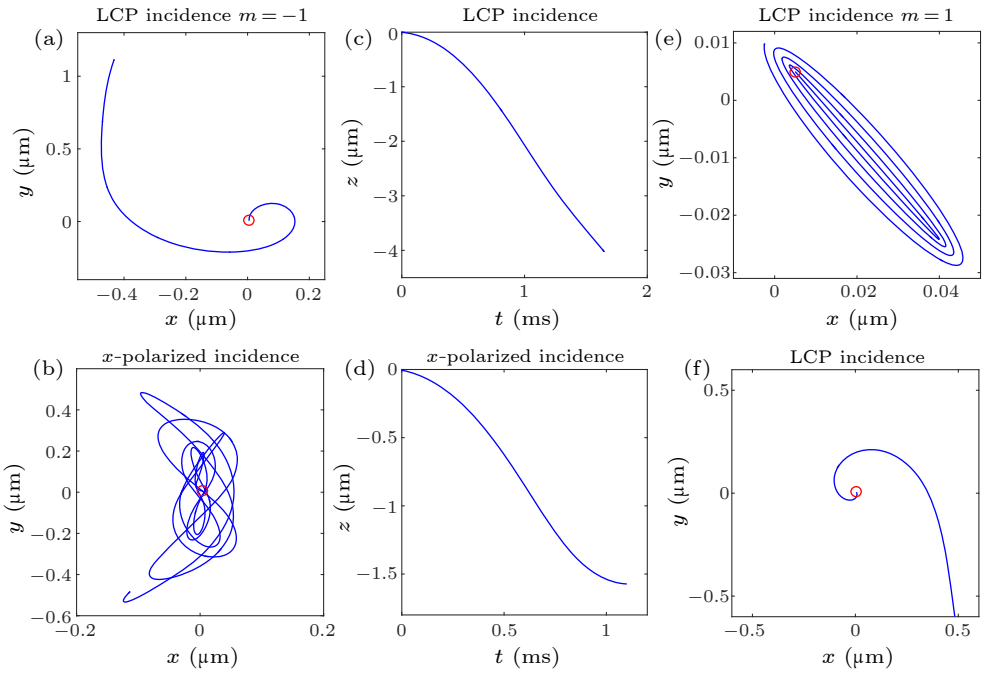

Fig. 6. (a) The x–y cross-sectional view of the particle trajectory with the incidence of an LCP beam. The red circle represents the starting point at (5 nm, 5 nm). (b) The particle trajectory with the incidence of the x-polarized beam. It should be noted that in order to show the trajectory more clearly, the scale of the abscissa and the ordinate of the figure are different. [(c), (d)] The displacement of particles along the z-axis under two incident beams. [(e), (f)] The x–y cross-sectional view of the particle trajectories in beams with vortex ($m = \pm 1$). The red circle represents the starting point at (5 nm, 5 nm). The titles of the figures indicate the polarization states of the incident beams.

In summary, we have designed polarization-insensitive metasurfaces for generation of non-paraxial Bessel beams with different polarization states. These tractor beams exert OPF on particles without the aid of background materials, and OPFs are sensitive to the radius of the particle. When the polarization states change, the radii of particles subjected to the pulling force will also change, which offers a possibility of the switch between pulling and pushing forces on a target particle, and it can also obtain the operation of particles in different spatial ranges. Meanwhile, when the topological charge changes, Bessel tractor beams have OPFs on particles with the disjoint ranges of radii. The possibility of a polarization-controlled particle sorting according to the particle size is indicated due to such features, and alternative methods to realize optical dynamic manipulation of nanoparticles are offered, which can be realized with the combination of the metasurfaces and the microfluidic system. The calculation of trajectory reveals that a particle with a specific radius can be pulled at a distance large enough to be identified by the tractor beam. Thus, our work has potential application in particle manipulation and finds the possibility in optical sorting, and can be used with rare or precious cell samples in nanoliter volumes without the need of complex microfluidic systems, and the setup of the metasurfaces can be used in the analysis of biomolecules, on-chip object transportation and optofluidic devices.

Acknowledgments. This work was supported by the National Natural Science Foundation of China (Grant Nos. 61805119 and 62275122), the Natural Science Foundation of Jiangsu Province (Grant Nos. BK20180469 and BK20180468), and the Fundamental Research Funds for the Central Universities (Grant No. 30919011275).

References

[1] Ashkin A 1970 *Phys. Rev. Lett.* **24** 156
[2] Zensen C, Villadsen N, Winterer F, Keiding S R, and Lohmuller T 2016 *Apl Photon.* **1** 026102
[3] Grier D G 2003 *Nature* **424** 810

[4] Ashkin A 2006 *Optical Trapping and Manipulation of Neutral Particles Using Lasers* (Hackensack, NJ: World Scientific)
[5] Dogariu A, Sukhov S, and Sáenz J 2013 *Nat. Photon.* **7** 24
[6] Shen Z, Xiang Z Y, Wang Z Y, Shen Y C, and Zhang B F 2021 *Appl. Opt.* **60** 4820
[7] Ahn J, Xu Z J, Bang J, Deng H Y, Hoang T M, Han Q K, Ma R M, and Li T C 2018 *Phys. Rev. Lett.* **121** 033603
[8] Koch M and Rohrbach A 2012 *Nat. Photon.* **6** 680
[9] Liu L R, Hood J D, Yu Y, Zhang J T, Hutzler N R, Rosenband T, and Ni K K 2018 *Science* **360** 900
[10] Righini M, Volpe G, Girard C, Petrov D, and Quidant R 2008 *Phys. Rev. Lett.* **100** 186804
[11] Chen J, Ng J, Lin Z, and Chan C T 2011 *Nat. Photon.* **5** 531
[12] Ding K, Ng J, Zhou L, and Chan C T 2014 *Phys. Rev. A* **89** 063825
[13] Novitsky A, Ding W Q, Wang M Y, Gao D L, Lavrinenko A V, and Qiu C W 2017 *Sci. Rep.* **7** 652
[14] Sukhov S and Dogariu A 2011 *Phys. Rev. Lett.* **107** 203602
[15] Nieto-Vesperinas M, Saenz J J, Gomez-Medina R, and Chantada L 2010 *Opt. Express* **18** 11428
[16] Brzobohaty O, Karasek V, Siler M, Chvatal L, Cizmar T, and Zemanek P 2013 *Nat. Photon.* **7** 123
[17] Ding W, Zhu T, Zhou L M, and Qiu C W 2019 *Adv. Photon.* **1** 024001
[18] Mizrahi A and Fainman Y 2010 *Opt. Lett.* **35** 3405
[19] Kajorndejnukul V, Ding W, Sukhov S, Qiu C W, Dogariu A 2013 *Nat. Photon.* **7** 787
[20] Petrov M I, Sukhov S V, Bogdanov A A, Shalin A S, and Dogariu A 2016 *Laser Photon. Rev.* **10** 116
[21] Lee S H, Roichman Y, and Grier D G 2010 *Opt. Express* **18** 6988
[22] Carretero L, Acebal P, Garcia C, and Blaya S 2015 *Opt. Express* **23** 20529
[23] Novitsky A, Qiu C W, and Wang H F 2011 *Phys. Rev. Lett.* **107** 203601
[24] Paterson L, Papagiakoumou E, Milne G, Garces-Chavez V, Tatarkova S A, Sibbett W, Gunn-Moore F J, Bryant P E, Riches A C, and Dholakia K 2005 *Appl. Phys. Lett.* **87** 123901
[25] Paterson L, Papagiakoumou E, Milne G, Garces-Chavez V, Briscoe T, Sibbett W, Dholakia K, and Riches A C 2007 *J. Biomed. Opt.* **12** 054017
[26] Mitri F G, Li R X, Guo L X, and Ding C Y 2017 *J. Quant. Spectrosc. Radiat. Transfer* **187** 97
[27] Pfeiffer C and Grbic A 2015 *Phys. Rev. B* **91** 115408
[28] Xie Z, Armbruster V, and Grosjean T 2014 *Appl. Opt.* **53** 6103
[29] Bowman R, Muller N, Zambrana-Puyalto X, Jedrkiewicz O, Di Trapani P, and Padgett M J 2011 *Eur. Phys. J. Spec. Top.* **199** 159
[30] Shen Z, Liu H C, Zhang S, Shen Y C, Zhang B F, Luo S Y 2019 *Appl. Opt.* **58** 5794
[31] Xiang Z Y, Shen Z, and Shen Y C 2022 *Sci. Rep.* **12** 1053
[32] Wen J, Chen L, Chen X, Kanwal S, Zhang L H, Zhuang S L, Zhang D W, and Lei D Y 2021 *Laser Photon. Rev.* **15** 2000487
[33] Fu R, Chen K, Li Z, Yu S, and Zheng G 2022 *Opto-Electron. Sci.* **1** 220011
[34] Zhang F, Pu M B, Li X, Gao P, Ma X L, Luo J, Yu H L, and Luo X G 2017 *Adv. Funct. Mater.* **27** 1704295
[35] Balthasar M J P, Rubin N A, Devlin R C, Groever B, and Capasso F 2017 *Phys. Rev. Lett.* **118** 113901
[36] Guo Y H, Zhang S C, Pu M B, He Q, Jin J J, Xu M, Zhang Y X, Gao P, and Luo X G 2021 *Light Sci. Appl.* **10** 63
[37] Bohren C F and Huffman D R 1983 *Absorption and Scattering of Light by Small Particles* (New York: Wiley)
[38] Khorasaninejad M, Chen W T, Devlin R C, Oh J, Zhu A Y, and Capasso F 2016 *Science* **352** 1190
[39] Zhan Q W 2009 *Adv. Opt. Photon.* **1** 1